Thermal Expansion of Fumed Silica/Cyanate Ester Nanocomposites

William K. Goertzen, M. R. Kessler

Department of Materials Science and Engineering, Iowa State University, Ames, Iowa 50011

Received 1 October 2007; accepted 2 January 2008
DOI 10.1002/app.28071
Published online 1 April 2008 in Wiley InterScience (www.interscience.wiley.com).

ABSTRACT: The thermal expansion behavior of a cyanate ester matrix reinforced by fumed silica nanoparticles with average primary particle diameters of 12 and 40 nm was investigated with thermomechanical analysis. All nanocomposites showed decreased coefficients of thermal expansion (CTEs) in comparison with the neat bisphenol E cyanate ester resin, but the 12-nm fumed silica nanocomposites had lower CTEs than the 40-nm nanocomposites for equal volume fractions. The largest decrease in CTE was 27.0% for 20.7 vol % 40-nm fumed silica. When the data were compared to applicable theory, the best fit of the data was given by Schapery's upper limit and Shi's model. Estimates of the interphase volume fraction and effective thickness surrounding the nanoparticles were made with the results of Shi's model, and the results showed that the interphase volume fraction was larger for the 12-nm fumed silica nanocomposites, given an equal fraction of silica. The glass-transition temperature of the nanocomposites from thermomechanical analysis varied only slightly with the volume fraction. © 2008 Wiley Periodicals, Inc. J Appl Polym Sci 109: 647–653, 2008

Key words: nanocomposites; silicas; thermal properties; thermosets

INTRODUCTION

The coefficient of thermal expansion (CTE) of polymers and polymer composites is an extremely important material property because of the relatively high CTE of polymers in comparison with other materials. Polymers are often filled with low-CTE or negative-CTE reinforcements to reduce the CTE mismatch in parts in which polymers are used in conjunction with other materials. Applications include electronic flip-clip underfills, electronic packaging, metal part replacement, coatings, and structural adhesives.[1–3]

There have been many studies on the reduction of the CTE of thermosetting polymers with inorganic fillers. The largest amount of literature on this subject concerns epoxies and polyesters, but there have also been many reports on the modification of high-temperature thermosets, such as cyanate esters, polyimides, and bismaleimides. Inorganic fillers used in thermosets include silica, zirconium tungstate (ZrW_2O_8), alumina, silicon nitride, aluminum nitride, functional polyhedral oligomer silsesquioxane (POSS), and layered silicates. Wooster et al.[4–6] reported on composites of cyanate esters and micrometer-sized fused silica, showing improved mechanical properties and reduced CTE for high loadings. Wippl et al.[3] investigated the reinforcement of high-temperature thermosets (bismaleimides, polyimides, and cyanate esters) with high loadings of fused silica, silicon nitride, and alumina, and CTEs as low as 15 ppm/°C were reported for volume fractions up to 80%. Wong and Bollampally[2] reinforced epoxy with silica, alumina, and silica-coated aluminum nitride and reported decreases in CTE of up to 65% with filler contents of 50% by volume. ZrW_2O_8, a unique ceramic with a strongly negative CTE over a wide temperature range, has shown potential for significant reduction of the CTE of composite materials with polymer matrices in both microparticulate and nanoparticulate form.[1,7,8] Shi et al.[1] investigated polyester and epoxy matrix composites with ZrW_2O_8, Weyer et al.[7] investigated ZrW_2O_8 with cyanate ester, and Sullivan and Lukehart[8] investigated the CTE reduction of micro- and nanoparticulate ZrW_2O_8/polyimide films. POSS has also been used for reduction of the CTE of thermosetting polymers. Significant decreases in the CTEs of epoxies and polyimides have been realized through the use of functionalized POSS.[9,10] Finally, layered silicate nanocomposites are another class of materials that can exhibit significant CTE reductions for epoxy and cyanate ester matrices.[11–13]

Correspondence to: M. R. Kessler (mkessler@iastate.edu).
Contract grant sponsor: National Science Foundation (through a graduate research fellowship)..
Contract grant sponsor: Strategic Environmental Research and Development Program (through the ''Environmentally Benign Repair of Composites Using High Temperature Cyanate Ester Nanocomposites'' project); contract grant number: WP-1580.

© 2008 Wiley Periodicals, Inc.
WILEY InterScience® DISCOVER SOMETHING GREAT

Fumed silica consists of amorphous silicon dioxide particles (between 7 and 40 nm in diameter) that are usually sintered together during the flame hydrolysis manufacturing process, which yields aggregates of the primary particles that are about 0.2–0.3 μm in diameter.[14] Although fumed silica has been used extensively with thermosetting polymers, such as polyesters,[15] polyurethanes,[16,17] and epoxies,[18–22] for the enhancement of processing and mechanical properties, there have been few studies on fumed silica's effect on CTE. Fumed silica should have a significant effect on a polymer's CTE because amorphous silicon dioxide has a CTE of only 0.75 ppm/°C.[23] Chung[24] reported a reduction in the thermal expansion of cement-based materials with added fumed silica in addition to other property enhancements such as increased mechanical properties, sag resistance, and improved filler fiber dispersion. For thermoplastic polymers, Fellahi et al.[25] showed that fumed silica reduced the CTE of rigid poly(vinyl chloride), and the use of coupling agents enhanced this effect.

The effect of fumed silica on the CTE of cyanate esters has not been reported. Even though the use of fumed silica with cyanate esters is mentioned in the patent literature for cyanate ester based adhesives,[26,27] there is a lack of literature on the reinforcement of cyanate esters with fumed silica. Other types of silica have been investigated with cyanate esters. Although POSS has shown potential for the reduction of CTE of epoxies and polyimides,[9,10] the reports on the use of POSS with cyanate esters do not cover thermal expansion.[28,29] As mentioned previously, micrometer-sized fused silica has been used with success in cyanate esters to reduce CTE.[4]

Here we report the effect that the particle size and volume fraction of fumed silica have on the thermal expansion behavior and glass transition of a cyanate ester matrix. The CTE data are compared to applicable theory for composite materials, and conclusions are made concerning the effect of the polymer–particle interaction. In parallel work, we investigated the effects of the particle size and volume fraction on other properties, such as rheology and curing kinetics[30] and mechanical properties.[31] In that work, we used dynamic mechanical analysis to show that the storage modulus increased with the volume fraction of fumed silica in both the glassy and rubbery regions, but the increase was more pronounced in the rubbery region. Furthermore, decreases in damping behavior were used to estimate the effective polymer–particle interphase thickness.[31]

EXPERIMENTAL

Materials

The bisphenol E cyanate ester (BECy) monomer used was a commercially available resin from Bryte Technologies (Morgan Hill, CA) called EX-1510. The liquid phase organometallic-based polymerization catalyst (EX-1510-B, Bryte Technologies) was supplied with the resin and was used at the manufacturer's suggested loading of 3 parts per hundred parts of resin (phr). The composition of the product is primarily bis(4-cyanatophenyl)-1,1-ethane monomer (or BECy), which has an extremely low viscosity, 0.09–0.12 Pa s, at room temperature.[32]

Hydrophilic fumed silica was supplied by Degussa (Frankfurt, Germany) under the trade names of Aerosil 200 and Aerosil OX 50 (CAS no. 112945-52-5, synthetic amorphous, pyrogenic silica, purity ≥ 99.8%, true density = 2.2 g/cm^3). Aerosil 200 has an average primary particle diameter of 12 nm and a specific surface area of 200 m^2/g.[33] Aerosil OX 50 has an average primary particle diameter of 40 nm and a specific surface area of 50 m^2/g.[33] The flame hydrolysis process used to make fumed silica yields mostly aggregates (primary particles sintered together) that are about 0.2–0.3 μm in diameter.[14]

Specimen manufacturing

BECy monomer/fumed silica suspensions were prepared by the addition of the fumed silica during the mixing of the monomer with a 25-mm-diameter high-shear blade at 1000 rpm. For the 12-nm particles, compositions of 0.5, 1, 2, 5, and 6.72 phr were made, with 6.72 phr (3.4 vol %) representing the maximum loading achieved with ease of processing. For the 40-nm particles, the compositions included 0.5, 1, 2, 5, 10, 20, 35, and 49.2 phr (maximum loading), representing volume fractions of up to 20.7 vol %. Before mixing, the fumed silica was dried *in vacuo*, and the BECy monomer was preheated to 60°C. The partially dispersed suspension was processed with a Fisher model 100 sonic dismembrator (Fisher Scientific, Pittsburgh, PA) with a 3.2-mm-diameter probe tip for 30 s at a frequency of 23 kHz. The power output ranged between 16 and 18 W during sonication. After sonication, the suspension was again mixed for 2 min at 2000 rpm, and this was followed by an additional 30 s of sonication. The temperature of the suspension was maintained between 50 and 65°C throughout the entire process. A predetermined amount of the catalyst was added to the dispersed suspension, corresponding to 3 phr, and mixed at 2000 rpm for 2 min; this was followed by 15 s of sonication at the same power level. Finally, the suspensions were poured into high-temperature silicone rubber molds (27 × 48 × 8 mm^3), degassed at 60°C for 1 h *in vacuo* at 23.4 mmHg, and then placed in a convection oven (preheated to 60°C) for the final curing process (heated to 180°C at 1°C/min, held for 2 h, heated to 250°C at 1°C/min, held for 2 h, and cooled to the

ambient temperature at 5°C/min). Samples were machined from the solid block of material with a diamond blade saw (TechCut 5 precision sectioning machine with a diamond wafering blade, low-concentration diamond metal bonded, 6″ × 0.020″ × 0.5″, Allied High Tech Products, Inc., Rancho Dominguez, CA). Specimens for thermomechanical analysis (TMA) were machined to 3 × 3 × 6 mm^3 so that the top and bottom faces of each specimen were parallel to within 15 μm. Neat BECy control samples without fumed silica were prepared in the same manner mentioned previously. All samples were dried at 120°C *in vacuo* for 6 h and kept in a dry environment before testing.

Experimental procedure

Thermomechanical testing was completed with a TA Instruments (New Castle, DE) TMA Q400. Samples were tested in the longest dimension (6-mm height) under a static force of 50 mN through two heating and cooling cycles from 30 to 300°C at a heating rate of 5°C/min under a helium purge at 50 mL/min. For each condition, multiple samples were tested (between 2 and 6), and the data were averaged. For measurements in which the standard deviation was more than the size of the symbol used in plots, error bars representing one standard deviation were included.

RESULTS AND DISCUSSION

Thermal expansion

Figure 1 shows an example of the raw data from the thermomechanical tests and the analysis performed on the data. Although the data in the first heating phase are dependent on the thermal and mechanical

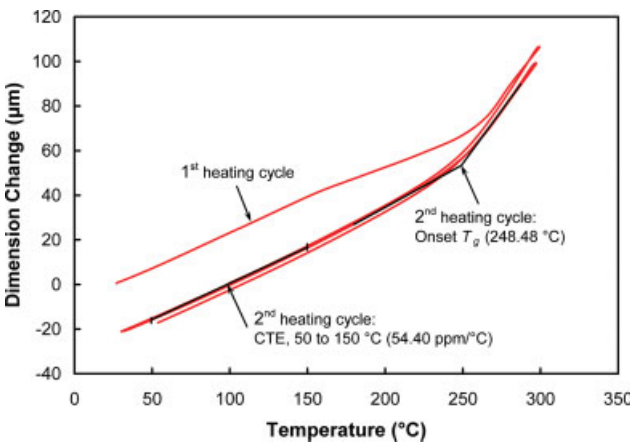

Figure 1 Example of raw TMA data with analysis (20 phr, 40-nm silica is shown). [Color figure can be viewed in the online issue, which is available at www.interscience.wiley.com.]

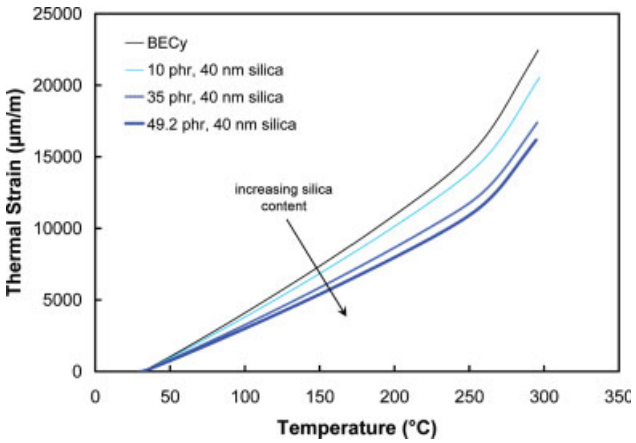

Figure 2 Strain versus the temperature for 40-nm fumed silica/cyanate ester nanocomposites. [Color figure can be viewed in the online issue, which is available at www.interscience.wiley.com.]

history of the specimen, the second heating phase provides information about the true material behavior only.[34] For this reason, the glass-transition temperature (T_g) and the CTE were taken from the second heating cycle. The CTE was calculated from the slope of the strain–temperature data in the region from 50 to 150°C. The strain is proportional to the dimension change (which is shown in Fig. 1) by the height of the specimen. Sample strain–temperature curves for the second heating cycle are shown in Figure 2 for the 40-nm nanocomposites at silica loadings of 0 (0.0 vol %), 10 (5.03 vol %), 35 (15.6 vol %), and 49.2 phr (20.7 vol %).

There is an obvious decrease in thermal strain with an increasing volume fraction of the filler material (ϕ_f). This is due to the influence of the low-CTE fumed silica. The CTE results for each volume fraction of both the 12- and 40-nm fumed silica nanocomposites are shown in Figure 3. As expected, the largest decrease in CTE was for the highest loading of 40-nm fumed silica (49.2 phr or 20.7 vol %), which reduced the BECy CTE by 27.0%, from 63.5 to 46.3 ppm/°C.

In Figure 3, the experimental CTE data are shown along with model predictions. Among the many different micromechanical models for the isotropic thermal expansion of composites, the simplest is the rule of mixtures (or mixed-law behavior):

$$\alpha_c = \alpha_f \phi_f + \alpha_m (1 - \phi_f) \quad (1)$$

where α_c, α_m, and α_f are the CTEs of the composite, matrix, and filler, respectively. The rule of mixtures is an approximation that does not consider the mechanical interaction between the phases. The rule of mixtures approximation yields the most conservative approximation for CTE because of an assumption of a constant stress in the two phases (isostress). In

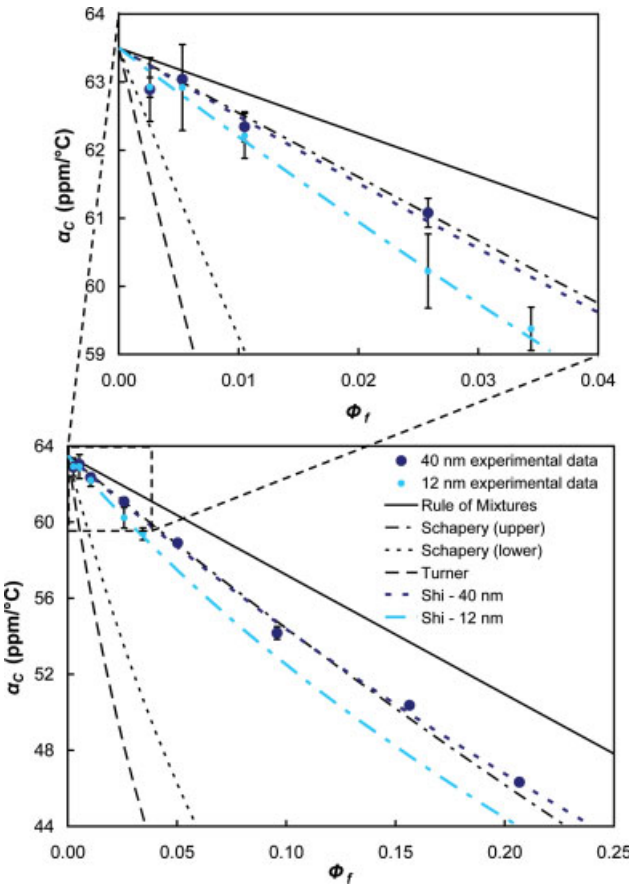

Figure 3 Experimental CTE versus the volume fraction data for fumed silica nanocomposites along with model predictions. [Color figure can be viewed in the online issue, which is available at www.interscience.wiley.com.]

contrast, Turner's model assumes equal dimension change with temperature for all phases, taking into account the interaction between the phases by assuming a constant strain throughout the two phases (isostrain). α_c becomes

$$\alpha_c = \frac{(1-\phi_f)K_m\alpha_m + \phi_f K_f \alpha_f}{(1-\phi_f)K_m + \phi_f K_f} \tag{2}$$

where K_m and K_f are the bulk moduli of the matrix and filler, respectively.[2] In general, Turner's model predicts very low CTE values and provides a lower limit for CTE. Turner's model is most applicable for unidirectional composites in the fiber direction.

Schapery[35] developed equations for the thermal expansion of composites using energy principles, giving upper and lower bounds to α_c. The upper and lower bounds for the isotropic CTE of the composite, α_c^u and α_c^l, respectively, are given by

$$\alpha_c^u = \alpha_m + \frac{K_f}{K_c^l}\frac{(K_m - K_c^l)(\alpha_f - \alpha_m)}{(K_m - K_f)} \tag{3}$$

$$\alpha_c^l = \alpha_m + \frac{K_f}{K_c^u}\frac{(K_m - K_c^u)(\alpha_f - \alpha_m)}{(K_m - K_f)} \tag{4}$$

where K_c^u and K_c^l are the upper and lower bounds of the bulk modulus of the composite material, respectively. These bounds, which are analogous to those derived by Hashin and Shtrikman,[2,37] assume dispersed constituents and are given by

$$K_c^u = K_f + \frac{1-\phi_f}{\frac{1}{K_m - K_f} + \frac{\phi_f}{K_f + \frac{4}{3}G_f}} \tag{5}$$

$$K_c^l = K_m + \frac{\phi_f}{\frac{1}{K_f - K_m} + \frac{1-\phi_f}{K_m + \frac{4}{3}G_m}} \tag{6}$$

where G_m and G_f are the shear moduli of the matrix and filler, respectively. The upper and lower bounds represent assumptions of isostress and isostrain behavior, respectively.

For both sets of data, the rule of mixtures approximation overestimates the CTE for all volume fractions, and this indicates that there is some strain transfer between the fumed silica and cyanate ester matrix. Schapery's lower limit and Turner's model underestimate the composite CTE for all volume fractions. These models are for an isostrain assumption and are reserved for composites with unidirectional or aligned reinforcement with significant aspect ratios. The experimental data for 40 nm, however, follow Schapery's upper limit very closely, and the 12-nm data lie slightly below Schapery's upper limit. Schapery's upper limit is likely the most applicable model because it gives results nearly identical to those of models for particulate-reinforced composites, such as those presented by Hashin and Shtrikman,[37] Kerner,[38] and Wang-Kwei.[39]

Because the rule of mixtures overestimates the composite CTE for the fumed silica/cyanate ester nanocomposites, there must be an interaction between the two phases that enables strain transfer and alteration of the properties of the matrix in close proximity to the filler. Shi's model is a modification of the rule of mixtures that includes an interphase region between the matrix and filler, and it is given by

$$\alpha_c = \frac{\alpha_f\phi_f + \alpha_m(1-\phi_f) + K_0\phi_f(1-\phi_f)(\alpha_f + \alpha_m) + K_0\phi_f(1-\phi_f)K_1}{1 + K_0\phi_f(1-\phi_f)} \tag{7}$$

where K_0 and K_1 are measures of the interphase that are approximated by the fitting of the model to experimental CTE data.[36] Curve fits to the experimental CTE data with Shi's model are also shown in Figure 3. For the 40-nm fumed silica nanocomposites, $K_0 = 0.58$ and $K_1 = -4.4$, and for the 12-nm nanocomposites, $K_0 = 1.1$ and $K_1 = -1.4$. From Shi's model, K_0 is related to the volume fraction of the interphase (ϕ_{int}) by

$$\phi_{int} = K_0 \phi_f \phi_m = \phi_f \frac{3\Delta R}{R}. \quad (8)$$

As given by eq. (8), K_0 is also related to the effective thickness of the interphase (ΔR) between the filler and matrix for particles with radius R.[36] When the constant K_0 is zero, rule of mixtures behavior is assumed; increasingly positive values of K_0 indicate a strong interaction between the filler and matrix.[36]

The constant K_1 is related to the CTE of the interphase (α_{int}) by

$$\alpha_{int} = K_1 + \alpha_f + \alpha_m - \alpha_c \quad (9)$$

so that a large negative value for K_1 indicates a strong interaction and a lowered value of α_{int}. Thus, for both the 12- and 40-nm nanocomposites, Shi's model predicts an interaction between the fumed silica and cyanate ester matrix such that predicted CTEs are lower than rule of mixtures behavior would suggest. For the fit of the data with each model, eq. (8) was used to estimate the effective thickness and volume fraction of the interphase between the particles and matrix. These results are tabulated in Table I.

TABLE I
Estimated Interphase Thickness (ΔR) and Volume Fractions (ϕ_f and ϕ_{int}) from Shi's Model

	ϕ_f	ϕ_{int}	ΔR (nm)
phr (12 nm)			
0.5	0.003	0.003	2.2
1	0.005	0.006	2.2
2	0.010	0.011	2.2
5	0.026	0.027	2.1
6.72	0.034	0.035	2.0
phr (40 nm)			
0.5	0.003	0.002	3.9
1	0.005	0.003	3.8
2	0.010	0.006	3.8
5	0.026	0.014	3.7
10	0.050	0.027	3.6
20	0.096	0.048	3.3
35	0.156	0.070	3.0
49.2	0.207	0.085	2.7

The average ΔR value for 12 nm is 2.1 nm; the average ΔR value for 40 nm is 3.5 nm.

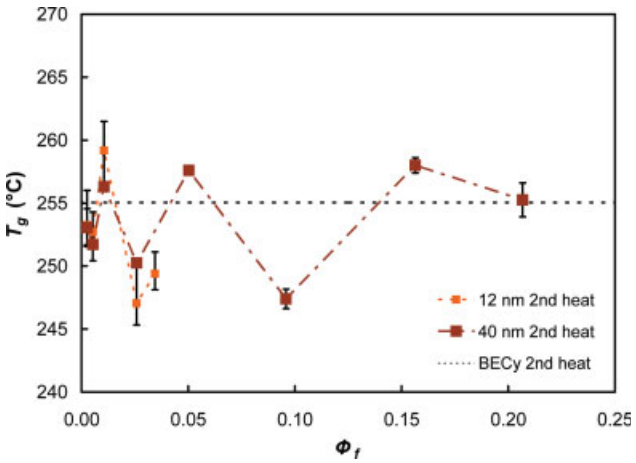

Figure 4 TMA T_g versus the volume fraction for 12- and 40-nm silica nanocomposites (the horizontal, dashed line indicates T_g of the neat BECy resin). [Color figure can be viewed in the online issue, which is available at www.interscience.wiley.com.]

According to the predictions, the interphase thickness is greater for the 40-nm fumed silica than for the 12-nm fumed silica. This is consistent with our observations made from dynamic mechanical damping experiments in our parallel work,[31] and the difference is attributed to less aggregation of the 40-nm nanoparticles allowing for more free surface area. However, because the 12-nm particles have a greater surface area per volume than the 40-nm particles, the overall interphase volume fraction is higher for the 12-nm nanocomposites. Because the interfacial interaction between the fumed silica and cyanate ester matrix is strong, the 12-nm nanocomposites with more surface area have lower CTEs than the 40-nm nanocomposites for the same volume fraction. The strong interaction between the polymer matrix and fumed silica is attributed to the formation of covalent linkages between the hydroxyl groups of the fumed silica and the cyanate group of the prepolymer matrix.[28]

Glass transition

Figure 4 shows the T_g values for the nanocomposites measured from the temperature at which the extrapolated glass and rubber lines cross in the second heating cycle of thermomechanical tests (as illustrated in Fig. 1). Initially, it does not appear that there is an obvious trend in T_g with an increasing silica volume fraction. However, the T_g's for the 12- and 40-nm samples follow the same trend, which indicates a source of systematic error because the samples with the same volume fraction were prepared at the same time. This error is attributed to the humidity of the laboratory on the day of sample

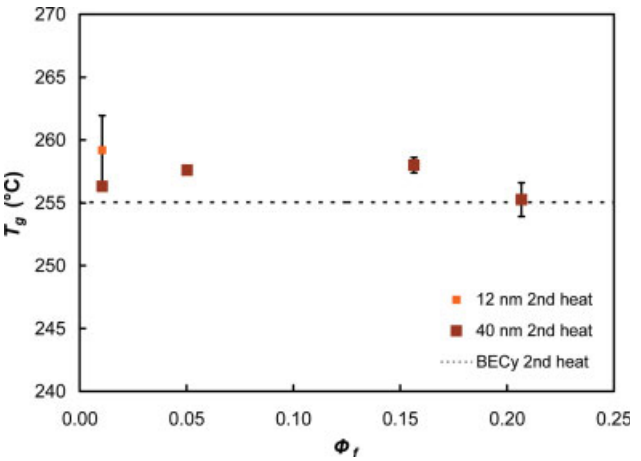

Figure 5 TMA T_g values for samples prepared under dry conditions. [Color figure can be viewed in the online issue, which is available at www.interscience.wiley.com.]

preparation (which varied from 19 to 60% relative humidity). If only samples prepared on days with a relative humidity of less than 20% are considered, T_g increases at every volume fraction (see Fig. 5). This trend was also seen in dynamic mechanical analysis glass-transition data in our parallel work,[31] and our hypothesis was confirmed by the preparation of identical samples under different environmental conditions and the monitoring of changes in T_g. It should be noted, however, that further testing showed that the CTE of the composites was not affected by changes in humidity. Additionally, neat BECy resin properties are not affected by environmental humidity because the monomer does not readily absorb moisture.

CONCLUSIONS

Cyanate esters reinforced with fumed silica particles of two different sizes showed decreased CTEs in comparison with the neat cyanate ester resin. The largest decrease in CTE was for the highest loading of 40-nm fumed silica (20.7 vol %), a composition that reduced the CTE of BECy by 27.0%, from 63.5 to 46.3 ppm/°C. For all compositions, the CTEs of the nanocomposites were lower than rule of mixtures predictions, indicating an interaction between the fumed silica and cyanate ester. Also, the 12-nm fumed silica nanocomposites had lower CTEs than the 40-nm nanocomposites of the same volume fraction, and this indicated that the increased surface area of the 12-nm fumed silica was effective in reducing CTE. The best model fit was provided by Schapery's upper limit, and a successful fit to the experimental data was also provided by Shi's model. From Shi's model, estimates of the interphase volume fraction and thickness were made, which indicated that although the thickness of the interphase surrounding the particles was less for the 12-nm nanocomposites than for the 40-nm nanocomposites, the overall volume fraction of the interphase was greater for the same volume fraction of fumed silica. The increased volume fraction of immobilized polymer around the nanoparticles was responsible for the further decrease in CTE for the 12-nm nanocomposites in comparison with the 40-nm nanocomposites. T_g of the nanocomposites was measured with TMA for all compositions, and the initial results showed no apparent trend in the data. However, the variation in T_g was linked to a source of systematic error: the level of humidity in the laboratory during sample preparation. In fact, all samples prepared under dry conditions evidenced at least minor increases in T_g.

The authors thank Ben MacMurray for his help with the preparation of the samples. Also, technical guidance from Xia Sheng, Jun Xu, and Mufit Akinc is greatly appreciated. This material is based upon work supported under a National Science Foundation Graduate Research Fellowship.

References

1. Shi, J. D.; Pu, Z. J.; Wu, K.-H.; Larkins, G. Proc Mater Res Soc Symp 1997, 445, 229.
2. Wong, C. P.; Bollampally, R. S. J Appl Polym Sci 1999, 74, 3396.
3. Wippl, J.; Schmidt, H.-W.; Giesa, R. Macromol Mater Eng 2005, 290, 657.
4. Wooster, T. J.; Abrol, S.; Hey, J. M.; MacFarlane, D. R. Compos A 2004, 35, 75.
5. Wooster, T. J.; Abrol, S.; Hey, J. M.; MacFarlane, D. R. Macromol Mater Eng 2004, 289, 872.
6. Wooster, T. J.; Abrol, S.; Hey, J. M.; MacFarlané, D. R. Macromol Mater Eng 2005, 290, 961.
7. Weyer, W. C.; Cross, W. M.; Henderson, B.; Kellar, J. J.; Kjerengtroen, L.; Welsh, J.; Starkovich, J. Proc AIAA/ASME/ASCE/AHS/ASC Struct Struct Dyn Mater Conf 2005, 6, 3577.
8. Sullivan, L. M.; Lukehart, C. M. Chem Mater 2005, 17, 2136.
9. Huang, J. C.; He, C.-B.; Xiao, Y.; Mya, K. Y.; Dai, J.; Siow, Y. P. Polymer 2003, 44, 4491.
10. Sulaiman, S.; Brick, C. M.; DeSana, C. M.; Katzenstein, J. M.; Laine, R. M.; Basheer, R. A. Macromolecules 2006, 39, 5167.
11. Kim, J.-K.; Hu, C.; Woo, R.; Sham, M.-L. Compos Sci Technol 2005, 65, 805.
12. Ganguli, S.; Dean, D.; Jordan, K.; Prire, G.; Vaia, R. Polymer 2003, 44, 1315.
13. Kim, D. S.; Lee, K. M. J Appl Polym Sci 2003, 90, 2629.
14. Cab-O-Sil® M-5 Product Technical Data; Cabot: Billerica, MA, 2000.
15. Lippe, R. J Mod Plast 1977, 54, 62.
16. Torro-Palau, A. M.; Fernandez-Garcia, J. C.; Orgiles-Barrelo, A.C., Martin-Martinez, J. M. Int J Ahes Adhes 2001, 21, 1.
17. Zhou, S.; Wu, L.; Shen, W.; Gu, G. J Mater Sci 2004, 39, 1593.
18. Miller, D. G. Adhes Age 1986, 29, 37.
19. Kang, S.; Hong, S.; Choe, C. R.; Park, M.; Rim, S.; Kim, J. Polymer 2001, 42, 879.

20. Preghenella, M.; Pegoretti, A.; Migliaresi, C. Polymer 2005, 46, 12065.
21. Jana, S. C.; Jain, S. Polymer 2001, 42, 6897.
22. Wichmann, M. H. G.; Cascione, M.; Fiedler, B.; Quaresimin, M.; Schulte, K. Compos Interface 2006, 13, 699.
23. ASM Engineered Materials Reference Book, 2nd ed.; Bauccio, M., Ed.; ASM International: Materials Park, OH, 1994.
24. Chung, D. D. L. J Mater Sci 2002, 37, 673.
25. Fellahi, S.; Boukobbal, S.; Boudjenana, F. J Vinyl Technol 1993, 15, 17.
26. Dershem, S. M.; Derfelt, D. L. U.S. Pat. 5,646,241 (1997).
27. Craig, W. M., Jr. U.S. Pat. 5,162,574 (1992).
28. Liang, K.; Li, G.; Toghiani, H.; Koo, J. H.; Pittman, C. U., Jr. Chem Mater 2006, 18, 301.
29. Liang, K.; Toghiani, H.; Guizhi, L. I.; Pittman, C. U. J Polym Sci Part A: Polym Chem 2005, 43, 3887.
30. Goertzen, W. K.; Kessler, M. R. Polym Eng Sci, to appear.
31. Goertzen, W. K.; Kessler, M. R. Compos A, to appear.
32. Shimp, D. A.; Craig, W. M., Jr. Proc Annu Int SAMPE Symp 1989, 34, 1336.
33. Aerosil® Product Technical Information; Degussa: Frankfurt, Germany, 2006.
34. Ehrenstien, G. W.; Riedel, G.; Trawiel, P. Thermal Analysis of Plastics: Theory and Practice; Hanser: Munich, 2004.
35. Schapery, R. A. J Compos Mater 1968, 2, 380.
36. Vo, H. T.; Todd, M.; Shi, F. G.; Shapiro, A. A.; Edwards, M. Microelectr J 2001, 32, 331.
37. Hashin, Z.; Shtrikman, S. J Mech Phys Solids 1963, 11, 127.
38. Kerner, E. H. Proc of the Physical Society: Section B 1956, 69, 808.
39. Wang, T. T.; Kwei, T. K. J Polym Sci A2 1969, 7, 889.